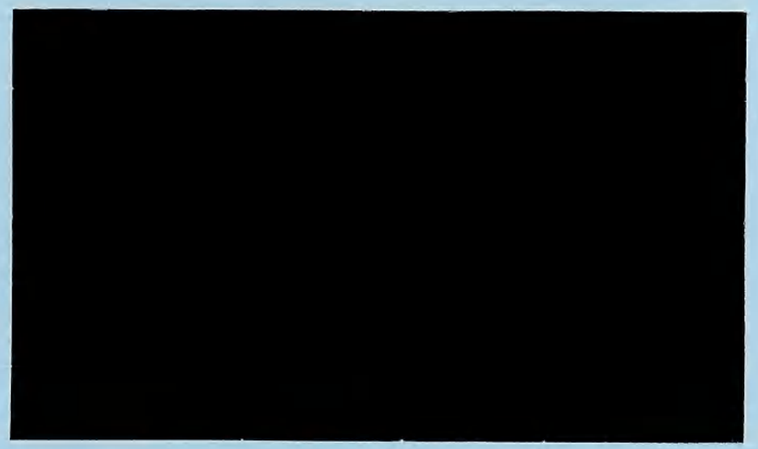

MAX-PLANCK-INSTITUT FÜR QUANTENOPTIK

Resonance absorption in a self-consistent streaming plasma

H. Takabe and P. Mulser

MPQ 49 July 1981

Max Planck-Institut
für Quantenoptik
BIBLIOTHEK
D-8046 Garching

D-8046 Garching bei München

Abstract

The plasma wave and the self-consistent density profiles are studied theoretically for resonance absorption of p-polarized laser light. The background plasma is assumed to flow in the stationary state in a plane geometry, the flow velocity varying from subsonic to supersonic near the critical density, and the Capacitor model is used. The enhanced plasma wave amplitude with its electron quivering velocity larger than the electron thermal velocity is induced for the driver strength $V_d/V_{th} > 0.1$. At the same time, in this regime the energy flux converted into the plasma wave is found to exceed the free-streaming limit of the electron heat flux. It is also found that hydrodynamic wave-breaking begins to play an essential role at $V_d/V_{th} \sim 0.7$.

1. Introduction

When a p-polarized electromagnetic wave is incident on an inhomogeneous plasma, resonance absorption occurs in the vicinity of the critical density, where the local plasma frequency is equal to the frequency of the incident wave. Physically, the absorption of the electromagnetic wave is caused by mode conversion of the electromagnetic wave into an electrostatic plasma wave. The actual irreversible dissipation is due to wave-particle interaction between the plasma wave and the electrons.
At the same time, it is well known that hot electrons are produced by collective acceleration by the wave field.
The hot electrons are recognized as the crucial element in achieving laser fusion because they preheat a fuel and generate fast ions. Investigating the properties of the plasma waves is significant because their structure directly affects the energy spectrum of the hot electrons.

On the other hand, it is also emphasized that the resonance absorption is strongly related to the density structure in the vicinity of the critical density. Especially at high-power irradiance, the ponderomotive force of the induced plasma wave (rather than the incident wave) is strong enough to modify the background plasma, and the steepened density profile with its scale

length of the order of a few times ten Debye lengths or less is formed. At the same time, this density modification influences plasma wave generation and hot electron production. Consequently, it has been agreed that investigation of the resonance absorption in conjunction with the self-consistent density is essential.

This subject has mainly been investigated by computational methods. The Particle-in-Cell codes [1),2),3)] have been used to study the dynamics of density modification, consistent fractional absorption, plasma waves causing tail formation in the electron distribution function, etc. Moreover, the scaling law of the hot electron temperature has been explained by comparing the experimental results with those from the PIC codes [4), 5)]. On the other hand, the density modification caused by plasma waves has been studied theoretically in Refs. 6 and 7 by solving the nonlinear Schroedinger equation with a driver term, interest being focused on the wave structure without treating wave-particle interaction. The study was done in the stationary rest plasma with a gentle gradient. The appearance of a caviton near the critical density was observed in the strong driver regime. For the self-consistent density in the presence of the background plasma flow, theoretical studies have been conducted in the case of s-polarization, where the density structure is consistent with the ponderomotive pressure of the electromagnetic

wave and the stationary state is assumed. The case of plane geometry was treated in Ref. 8, where the flow velocity is assumed to vary from subsonic to supersonic through the system, while in Ref. 9 this subject is treated on the assumption of supersonic flow in a spherical geometry.

In the laser fusion scheme, the plasmas interacting with the laser light expand into the vacuum region with the flow velocity of the order of the sound velocity. In investigating resonance absorption in the laser plasma, therefore, it is essential to treat it in the streaming plasma. In the present paper, the plasma wave and density structures for the p-polarized case are studied theoretically in the flowing plasma. For the p-polarized case, this calculation is very difficult because the actual mode is a mixed electromagnetic-electrostatic wave. However, adopting the Capacitor model makes the situation somewhat easier. Similar to the case in Ref. 8, the plasma flow with its velocity varying from subsonic to supersonic is assumed to be in a plane geometry. The equation of the plasma wave is solved self-consistently with the plasma flow profile, but the dissipation of the wave is not included self-consistently.

Solving the wave equation in conjunction with the ion fluid momentum equation yields two different kinds of solutions according to the different boundary conditions of the underdense region. That is, one consists of the density

profile monotonically decreasing along the flow and the other is formed with the density having a caviton in the overdense subsonic region. The former is obtained for the case of non-reflection at the underdense boundary, while the latter corresponds to the case with partial reflection there. As a typical example, the amplitude of the plasma wave is found to be enhanced by 6 times and 10 times the driver amplitude for the former and latter cases, respectively, at $V_d/V_{th} \sim 0.3$, where V_d is the quivering velocity of the electron due to the driver field and V_{th} is the electron thermal velocity. At the same time, the density scale length is seen to be steepened about 10 Debye lengths at the critical density by the ponderomotive force of the plasma wave.

As for the former with the monotonically decreasing density profile, the scaling laws are studied for the induced wave amplitude, density scale length, and the densities at the upper and lower density shelves by varying the driver strength. The enhanced wave amplitude with its electron quivering velocity larger than the thermal velocity is obtained for the relatively strong driver regime $V_d/V_{th} > 0.1$. Associated with the limiting condition for applying the present linear wave model to resonance absorption, the wave-breaking condition is estimated, and it is found that the wave breaks for $V_d/V_{th} \gtrsim 0.7$ in the sense of hydrodynamic wave-breaking. The energy conversion rate to the plasma wave is studied in relation to absorption. The energy flux converted into the plasma wave

is found to exceed the free-streaming heat flux of the background electron at the critical density for $V_d/V_{th} > 0.1$. It is also pointed out that the hot electrons are expected to appear in the same range, $V_d/V_{th} > 0.1$, from the simple standing-wave model.

In Sec. 2, the basic equations for the wave field and the background density are derived on the basis of the Capacitor model. The boundary conditions and assumptions in solving the wave equation are mentioned in Sec. 3. In this section, the wave equation is solved by introducing the analogy of the wave equation to the Newton equation in a two-dimensional potential field. In Sec. 4, the scaling laws for the various quantities scaled with the driver strength are investigated as well as the wave-breaking condition. Finally, Section 5 contains the summary and conclusion.

2. Basic Equations for Plasma Wave

As is well-known, in an expanding inhomogeneous plasma p-polarized electromagnetic waves induce plasma waves at the critical density by the linear-mode-conversion process. To describe this resonance absorption in a hot plasma, use is made of the linearized electron momentum equation combined with Maxwell's equations. The ion motion is assumed to be negligible for high-frequency responses:

$$m n_0 \frac{\partial}{\partial t} \mathbb{V} = -e n_0 \mathbb{E} - \gamma T_e \nabla n - m n_0 \nu_L \mathbb{V} , \quad (1)$$

$$\nabla \mathbb{E} = -4\pi e n , \quad (2)$$

$$\frac{\partial}{\partial t} \mathbb{E} = c \nabla \times \mathbb{B} + 4\pi e n_0 \mathbb{V} , \quad (3)$$

$$\frac{\partial}{\partial t} \mathbb{B} = -c \nabla \times \mathbb{E} , \quad (4)$$

where n_o is the background plasma density; T_e, m, and e are the electron temperature, mass, and charge, respectively; c is the velocity of light; and γ is the ratio of specific heats and is chosen equal to 3.

In eqs. (1)-(4), $\mathbb{V}$ and n are the electron velocity and density, and $\mathbb{E}$ and $\mathbb{B}$ the electric and magnetic fields, respectively.

In eq. (1), the effective collision fequency is introduced with ν_L, which is finite for the electrostatic motion but is assumed to be zero for the electromagnetic component. This procedure is taken from Ref. 2. The effect of the ambipolar field arising from the density inhomogenity is neglected here.

Inserting eq. (2) into eq. (1) and eq. (4) into eq. (3), and assuming the fields to vary as $e^{-i\omega t}$, where ω is the frequency of the external field, we obtain the steady-state wave equation for the electric field after combining eq. (1) and eq. (3):

$$\frac{\lambda_{DC}^2}{1+i\nu_L/\omega} \gamma \nabla^2 \mathbb{E} + \epsilon \mathbb{E} = \lambda^2 \nabla \times \nabla \times \mathbb{E} , \quad (5)$$

where $\lambda_{DC} = (T_e/m)^{1/2}/\omega$ is the Debye length at the critical density, $\lambda = c/\omega$ the wavelength of the electromagnetic wave in vacuum, and $\epsilon = 1 - \omega_p^2/\omega^2$ the dielectric of the cold plasma with the plasma frequency $\omega_p = (4\pi n_o e^2/m)^{1/2}$.

In the situation where the plasma waves are resonantly induced at the critical density, the electric field in eq. (5) is mainly attributed to the longitudinal component there without the L.H.S., which plays the role of the electromagnetic driver to the plasma waves. For such a case, eq. (5) can be reduced to the equation for the Capacitor model in the vicinity of the critical density,

as long as the skin depth $\lambda_s = c/\omega_p$ is sufficiently larger than the Debye length $\lambda_D = v_{th}/\omega_p$, i.e. $v_{th} \ll c$:

$$\frac{\lambda_{Dc}^2}{1+i\nu/\omega}\gamma\frac{d^2}{dz^2}E + \epsilon E = -i\lambda(\nabla\times B)_z \quad (\equiv E_d), \tag{6}$$

where $(\nabla\times B)_z$ denotes the Z-component of $\nabla\times B$, and the R.H.S. is assumed constant in Z and replaced by E_d for simplicity of notation.
In reducing eq. (5) to eq. (6), we have assumed the background plasma density is inhomogeneous in Z and the plasma waves propagate in this direction with the field $E = (0,0,E(Z))$.

In order to determine the wave structure by solving eq. (6), it is necessary to determine the background plasma density n_o self-consistently (because $\epsilon = 1 - n_o/n_{cr}$). For this purpose, we consider the situation where there is no external force and the system is self-sustaining owing to the balancing of the ion flow momentum and electron pressure with the ponderomotive force of the plasma waves. The background plasma density then remains inhomogeneous because the ion flow velocity varies from subsonic to supersonic as described below. From Ref. 8 the equations to the background plasma density are

$$n_o \cdot u_o = \text{const}, \tag{7}$$

$$m_i u_o \frac{d}{dz}u_o = -\frac{T_e}{n_o}\frac{d}{dz}n_o - \frac{m}{4}\frac{d}{dz}|V_{os}|^2, \tag{8}$$

where u_o is the flow velocity of the ion fluid and $V_{os} = \frac{e}{m\omega}E$ is the electron quivering velocity. In eqs. (7) and (8) quasi-neutrality ($\langle n_e\rangle = n_o$, where $\langle n_e\rangle$ is the time-averaged electron density), was assumed because the density scale length is still larger than the Debye length.

Substituting eq. (7) in eq. (8) and rewriting eqs. (6) and (8) in the normalized forms yield

$$(1+i\delta)^{-1}\frac{d^2}{d\xi^2}A + \left(1-\frac{\rho_s}{M}\right)A = A_d, \tag{9}$$

$$\left(M-\frac{1}{M}\right)\frac{d}{d\xi}M = -\frac{1}{4}\frac{d}{d\xi}|A|^2, \tag{10}$$

where

$$A = V_{os}/V_{th}, \quad M = u_o/C_s, \quad \xi = Z/\sqrt{\gamma}\lambda_{Dc},$$

$$\rho_s = n_s/n_{cr}, \quad A_d = V_d/V_{th}, \quad \delta = \nu_i/\omega,$$

where $V_{th} = (T_e/m)^{1/2}$ is the electron thermal velocity, $C_s = (T_e/m_i)^{1/2}$ the ion sound velocity (m_i ; ion mass), $V_{os} = \frac{e}{m\omega}E$ the electron quivering velocity by the driver field, and n_s the background plasma density at the sonic point. In eq. (9) the driver A_d is assumed to be real. Integrating eq. (10) from the sonic point (M = 1) to an arbitrary point gives the following relation between the Mach number M and the wave energy density $|A|^2$:

$$M^2 - \ln M^2 - 1 = \frac{1}{2}(A_s^2 - |A|^2), \qquad (11)$$

where A_s is the value of $|A|$ at the sonic point and $|\ |$ denotes taking an absolute value. The relation between M and $|A|^2$ in eq. (11) is depicted in Fig. 1. It should be noted that although the Mach number M is given as a function of $|A|^2$ with eq. (11), M has two solutions in subsonic ($M < 1$) and in supersonic ($M > 1$) regions corresponding to the same value of $|A|^2$. In the following, eq. (9) is solved with the aid of eq. (11) under appropriate boundary conditions.

3. Resultant Wave Structures

In order to determine the wave structure and the corresponding plasma profile, it is necessary to specify the appropriate boundary conditions on the wave equation (9). Since, in our model, the plasma density is higher than the critical density in the over dense region ($\xi \ll 0$), the plasma waves should attenuate there. The boundary condition at $\xi = -\infty$ is therefore $dA/d\xi = 0$. On the other hand, in the underdense region ($\xi \gg 0$), where the plasma density is lower than the critical density, the waves are assumed to be outgoing ones and attenuate as ξ increases because of the damping ν_L. The boundary condition for $\xi = \infty$ is therefore $dA/d\xi = 0$, too. In addition to these boundary conditions, the restrictive condition should be satisfied at the sonic point ($\xi = 0$) [8]. That is, as apparent from eq. (10), the amplitude of the electric field should be maximum at the sonic point; $d|A|/d\xi = 0$ at $\xi = 0$ where $M = 1$, in order for the flow velocity to vary smoothly across the sonic point. This imposes an additional condition on our problem. For these boundary conditions, in principle, eq. (9) provides a unique solution. And the unknown values ρ_s and A_s are determined in the sense of an eigenvalue problem for a given value A_d. Before solving eq. (9) directly, however, let us see its properties below.

In order to provide visible images, it is instructive and convenient to introduce the analogy of the wave equation with Newton equation of a point mass motion. In eq. (9) let us set $\delta = 0$ and $A = X + iY$, where X and Y are real and introduce a two-dimensional vector coordinate $\mathbb{R} = (X,Y)$. Using eq. (11), the wave equation (9) is then rewritten in the form

$$\frac{d^2}{d\xi^2}\mathbb{R} = -\frac{\partial}{\partial \mathbb{R}} U(\mathbb{R}) , \qquad (12)$$

$$U = U_s - A_d X ,$$

where

$$U_s = \frac{1}{2}(X^2+Y^2-A_s^2) + 2\rho_s\left(M+\frac{1}{M}-2\right). \qquad (13)$$

It is obvious that eq. (12) is the Newton equation of a point mass in the two-dimensional potential $U(\mathbb{R})$ if ξ is regarded as a real time. It is noted that the potential U consists of the symmetric component U_s and the asymmetric one $A_d \cdot X$. The structure of U_s is shown schematically in Fig. 2 for the subsonic case (Fig. 2(a)) and the supersonic case (Fig. 2(b)) by using eq. (11) to eliminate M in eq. (13). Note that in the subsonic case the potential has a hump at the centre only when the condition $\rho_s < 1$ is satisfied.

In the absence of the driver ($A_d = 0$), the wave structure giving subsonic-to-supersonic transition can be obtained by the solution corresponding to the particle path (1-2-3 in Fig. 2, and after arriving at the point "3" the path shows the oscillation between "2" and "3"). The wave corresponding to this path is a standing wave since the angular momentum of the point mass corresponds to the wave momentum in our analogy and the above path has no angular momentum. This is the solution obtained previously in Ref. 8, where an s-polarized electromagnetic wave is treated instead of our electrostatic wave.

On the other hand, in the case with finite A_d, the potential structure is deformed in the x-direction. The top of the potential hump, which is the equilibrium point and corresponds to the boundary at $\xi = -\infty$, is then shifted in the negative x-direction. It is obvious that the deformation of the potential helps the point mass starting from the equilibrium point to obtain an appropriate amount of angular momentum.

In the present paper, the following two assumptions are employed in solving eq. (9).

The first concerns the damping coefficient. In the situation where the large-amplitude plasma wave is ex-

cited with its quivering velocity nearly equal to the thermal velocity, the nonlinear wave-particle interaction determines the local damping rate and studying its actual value becomes one of the important problems. However, we do not go into detail beyond adopting an artificial, constant damping rate. Moreover, in the subsonic region we assume there is no damping. In this region the variation of the electric field of the wave is mainly in amplitude but not in phase, and the effective phase velocity is sufficiently large. The wave may not be subject to strong damping due to wave-particle interaction in the subsonic region. But, in the supersonic region, where the wave phase changes rapidly with the relatively small phase velocity, a sufficient damping rate is assumed.

The second assumption is adopted in order to simplify the eigenvalue problem. In the supersonic region the variation of M^{-1} in eq. (9) is neglected and M is set equal to unity. This assumption does not cause any essential change in the present problem since the density at the sonic point is smaller than the critical density: $\rho_s < 1$. The solution of eq. (9) in the supersonic region is then obtained analytically as

$$A = A_0 e^{i\kappa\xi + i\theta_0} + A_d/(1-\rho_s), \qquad (14)$$

where $\kappa^2 = (1-\rho_s)(1+i\delta)$ with $\mathrm{Re}(\kappa) > 0$, and A_0 and θ_0 are real constants.

With these assumptions, we reduce the present problem to solving eq. (12) in the subsonic region. Using the continuity conditions of the value and derivative of the electric field A at the sonic point, the constants A_0 and θ_0 in eq. (14) can be written in terms of A_d, ρ_s, and A_s. At the same time, the property of energy conservation of the "point mass" in the subsonic region for eq. (12),

$$\Delta U = \frac{1}{2}\left|\frac{dR}{d\xi}\right|^2\Big|_{\text{at sonic point}},$$

where ΔU is the potential difference between the equilibrium point ($\xi = -\infty$) and the sonic point ($\xi = 0$), provides an additional equation for A_d, ρ_s, and A_s. One of these three values is then eliminated. In the present paper, ρ_s has been eliminated and eq. (12) has been solved as the eigenvalue problem with the eigenvalue A_d for given A_s.
The integral of eq. (12) was carried out by starting from the sonic point (so-called shooting method) with the aid of the sixth-order Runge-Kutta method [10].

In Fig. 3, the resultant profiles are shown for the case with $A_s = 2$ and $\delta = 0.2$. The structures of the density (ρ_s/M) and ponderomotive

potential ($\Phi = |A|^2/4$) are shown in Fig. 3(a). The spatial profile of the wave (the real and imaginary parts of A) is depicted in Fig. 3(b), while its profile in the phase diagram is depicted in Fig. 3(c). The driver strength $A_d = 0.32$ is obtained and the related values are found to be $\rho_s = 0.39$, $\rho_1 = 1.54$, and $\rho_2 = 0.19$, where ρ_1 and ρ_2 are the upper and lower densities, respective. It should be noted that at the sonic point the amplitude of the plasma wave is enhanced about 6 times the driver strength and a sharp density gradient [$(d \ln n_o/dz)^{-1} \sim 10 \cdot \lambda_{DC}$] appears owing to the ponderomotive force of the plasma wave.

Although no reflection has been assumed at $\xi = \infty$ so far, the wave structure with a caviton in the subsonic region can be obtained by allowing partial reflection from the underdense region. The profiles shown in Fig. 4 are the result for $A_s = 3$ and $\delta = 0$ with 20 % reflection. For this case, the driver strength is found to be $A_d = 0.30$. The enhancement of the wave amplitude at the sonic point is 10, and this value is larger than the previous value for the case without cavitons in spite of almost the same driver strength. This is due to the fact that the caviton plays the role of the emitter, in which the wave is nearly a standing wave as seen from Fig. 4(c). Studying the properties of the wave with cavitons [11] is important and interesting, but in this paper we do not enquire further into this type of solution.

4. Resultant Scaling Laws

In this section, the scaling laws for the case corresponding to Fig. 3 are studied by varying the value of A_d with fixed damping rate $\delta = 0.1$. First, the maximum amplitude of the plasma wave at the sonic point ($V_{os,p}$) and the density scale length at the critical point (L_{cr}) are scaled with the applied driver strength in Figs. 5(a) and (b), respectively. They are found to be scaled, respectively, as

$$V_{os,p} \sim 3.5 \left(\frac{V_d}{V_{th}}\right)^{1/2} \cdot V_{th} , \qquad (15)$$

$$L_{cr} \sim 4 \cdot \left(\frac{V_d}{V_{th}}\right)^{-3/4} \lambda_{Dc} . \qquad (16)$$

These resultant scalings show, for example, that for $V_d/V_{th} = 0.5$ the ponderomotive pressure of the wave is enhanced about 25 times that of the driver field and the density scale length is steepened up to about 7 times the Debye length. Such steepened density scale lengths have also been observed in simulation plasmas [3), 4)].

As is well-known, the Airy function [3)] has been used as a solution of the mode conversion in hot plasmas with linear density gradient as long as its density scale length is much larger than the Debye length. The wave profile is then given in the form

$$A' = -\pi [G_i(\gamma) + i A_i(\gamma)] , \qquad (17)$$

where $A' = \varepsilon^{2/3} V_{os}/V_d$, $\eta = \varepsilon^{-2/3} z/L$, $\varepsilon = \sqrt{3} \cdot \lambda_{DC}/L$, and G_i and A_i are the Airy functions defined in Ref. 12. This solution yields the following scalings to the maximum amplitude of the plasma wave:

$$V_{os,p} = 1.3 \left(\frac{L}{\lambda_{DC}}\right)^{2/3} V_d \ , \qquad (18)$$

for the given density scale length L.
Inserting the self-consistent scale length L_{cr} obtained in eq. (16) into eq. (18) yields

$$V_{os,p} = 3.1 \left(\frac{V_d}{V_{th}}\right)^{1/2} V_{th} \ ,$$

which is in reasonable agreement with eq. (15). It may be concluded from this consideration that although the density profile is strongly modified from the idealized linear one and its scale length is no longer sufficiently large compared with the Debye length, the Airy function gives the appropriate amplitude for the resonantly induced plasma wave.

On the other hand, let us consider the self-consistent density scale length which is determined with the simple pressure balance between the wave pressure and the plasma pressure. Simply balancing these pressures, i.e. $T_e \nabla n_o = 1/4\ m\ n_o \nabla |V_{os}|^2$, with the aid of the wave structure given by eq. (17) yields

$$L = 3.7 \left(\frac{V_d}{V_{th}}\right)^{-1} \lambda_{DC} \ .$$

This scaling obtained with the simple pressure balance does not fit the self-consistent one given in eq. (16), possibly indicating contributions from the momentum of the plasma flow.

In Fig. 6, the densities of the upper and lower shelves are plotted as a function of the driver strength V_d/V_{th}, as well as the density at the sonic point. If we compare the present results with those obtained in the s-polarized case [8], it is clear that the density jumps are enhanced in the p-polarized case because of the predominant ponderomotive force of the plasma wave, where we have set $V_d = V_o$ in Ref. 8 to compare the two cases.

In the present paper, the wave is assumed to be linear and the fluid description, which neglects electron trapping and/or so-called wave-breaking,[13] is used. However, they come to play an important role in the wave phenomena as the plasma wave amplitude increases. Moreover, they play an essential role above some critical value of the driver strength. In order to estimate this critical value, the peak amplitude of the perturbed electron density is scaled in Fig. 7. It is seen that the peak value of $\delta n/n_o$ approaches unity at $V_d/V_{th} \sim 0.7$. Wave-breaking then occurs, where the electron oscillation velocity is nearly equal to the phase velocity of the plasma wave, and crucial trapping of the electrons by the wave potential occurs [14]. In such a situation, the electrons, which should sustain regular motions consisting of the wave, are subject to nonlinear interaction with the wave field, thus causing a strong dissipation to the wave. Consequently, it may be concluded that for the stronger driver

$V_d/V_{th} > 0.7$ the strong wave dissipation caused by wave breaking prevents the increase of the wave amplitude from following eq. (15) and a new scaling appears.

In addition to wave-breaking, it also becomes important to take into account the following two effects for such a strong driver regime. First, the ambipolar field induced by steepening of the plasma density with its scale length of several Debye lengths begins to play a role in reducing the wave amplitude. Second, the reactive force arising from the nonlinearity of the dispersion term in the electron momentum equation weakens the usual ponderomotive force,because the effective ponderomotive force consists of two terms in hot plasmas, i.e. $F_{NL} = - \langle mV \frac{\partial}{\partial x} V \rangle + T_e/n_o \langle \delta n \frac{\partial}{\partial x} \delta n \rangle$, where $\langle \quad \rangle$ denotes taking the time average over rapid oscillations, and the second term represents an additional force with the opposite sign to the first one.

Let us now see how much energy is converted into the plasma wave by mode conversion in the present model. From eqs. (1) - (4) the equation for the wave energy can be obtained in the conservative form

$$\frac{\partial}{\partial t}\left(\frac{E^2}{8\pi} + \frac{m}{2} n_0 V^2 + \frac{\gamma T_e}{2 n_0} n^2 \right) + \frac{\partial}{\partial z}(\gamma T_e n V) = i \frac{\omega}{4\pi} E_d \cdot E . \qquad (19)$$

In eq. (19), the L.H.S. shows a conservative form with the terms of the energy density and flux, while the R.H.S. denotes the coupling between the driver and the plasma wave. In the stationary situation the first term on the L.H.S. vanishes, and the energy converted into the plasma waven can be calculated as the energy flux at the boundary of the interaction region. Using eqs. (1) - (4), this energy flux can be rewritten as

$$Q_w = \gamma T_e n V \Big|_{\text{at sonic point}} = Q_c \frac{\sqrt{\gamma/2}}{\rho_s} \left(A_r \frac{d}{d\xi} A_i - A_i \frac{d}{d\xi} A_r \right), \qquad (20)$$

where $Q_c = n_{cr} T_e V_{th}$ is the free-streaming heat flux of the cold plasma at the critical point. In obtaining eq. (20), we have assumed that the boundary of the interaction region corresponds to the sonic point, where the plasma wave amplitude shows its maximum, and that $A_d^2 \ll A_s^2$ there. In eq. (20), A_r and A_i are the real and imaginary parts of the normalized wave field A at the sonic point. In Fig. 8, the normalized energy flux Q_w/Q_c is plotted as a function of the driver strength. This figure indicates that for the strong driver $V_d/V_{th} > 0.1$, the energy flux more than the cold electron free-streaming value Q_c is converted into that of the plasma wave.

In Fig. 8, on the other hand, the absorbed energy flux estimated with the local absorption model, which gives it in the form $Q_1 = 1/8 \cdot \omega L \cdot E_d^2$, is also plotted with dotted lines as a reference, where eq. (16) is used to estimate L in Q_1 . Since the ponderomotive force of the plasma wave determines the density structure, the interaction region ΔZ is almost equal to the density scale length L in the present model. Consequently, the local absorption model, which provides a well-approximated absorption rate for $\Delta Z \ll L$, does not fit the present result, as is obvious from Fig. 8.

Finally, let us briefly consider the possible hot electron temperature associated with the resultant waves. For this purpose, use is made of the results obtained in Ref. 15, where the plasma wave is modelled as a Gaussian--shaped standing wave. Although in the present case the wave is propagating, its phase velocity is larger than the electron oscillation velocity and thermal velocity in the range of $V_d/V_{th} < 0.7$. Consequently, the assumption of a standing wave may provide an appropriate hot electron temperature T_h. Using the resultant formula, $T_h/T_c = 0.6 + 12.5 \cdot \mathcal{E} \cdot \lambda_{DC}/D$, which is deduced from Fig. 5 in Ref. 15 and where $\mathcal{E}$ is the peak amplitude of the wave divided by the electron thermal velocity, and D is the width of the wave, the hot electron temperature to be expected is plotted in Fig. 9. In estimating T_h using the

above formula, $V_{os,p}/V_{th}$ and L_{cr} in eqs. (15) and (16) are used for $\mathcal{E}$ and D, respectively. From this figure it is found that the hot electrons with $T_h/T_c \sim 8$ are generated for $V_d/V_{th} \sim 0.7$ by the resonance wave with $\mathcal{E} \cdot \lambda_{DC}/D \sim 0.37$.

5. Summary and Conclusion

The properties of the plasma waves generated by resonance absorption have been investigated in a self--consistently streaming plasma. The ponderomotive force of the plasma waves is assumed to be balanced by the dynamic force arising from variation of the ion flow velocity from subsonic to supersonic across the resonance surface, and no external, artificial field is assumed to sustain the density inhomogeneity. The Capacitor model was adopted for modelling the wave generation in the p-polarized case. The results show that two types of solution can be obtained according to the different boundary conditions, i.e. the plasma wave with a caviton in the subsonic region for the reflective boundary in the lower density region, and that without a caviton for the non-reflective boundary there. For the cases without caviton formation, the scaling laws were investigated by varying the strength of the driver field.

The amplitudes of the generated plasma waves and the corresponding density scale length of the background plasmas were obtained in eqs. (15) and (16), respectively, as functions of the driver strength. The plasma wave with its wave energy larger than the electron thermal energy, $(V_{os}/V_{th})^2 > 1$, is found to be induced by the driver with relatively small amplitude, $V_d/V_{th} < 1$. At the same time,

the plasma density is steepened in the vicinity of the critical density with the scale length of 5 $\sim$ 10 Debye lengths. Moreover, the upper density shelf is formed by the ponderomotive force and its density is found to reach 2 times the critical density.

Associated with the applicability of the present linear model to the plasma wave, it is pointed out that wave-breaking begins to play a crucial role in the wave phenomena at the relatively strong driver $V_d/V_{th} \sim 0.7$. Setting $E_d^2 = \alpha E_o^2$, where E_o is the electric field of the laser in vacuo and α is a constant of order unity, yields this critical value for the wave-breaking in the form $I\lambda_L^2 \sim 1.2 \times 10^{15} \cdot T_e/\alpha$ [W/cm^2 $\cdot$ μm^2], where I is the laser intensity, λ_L its wavelength in μm, and T_e the temperature of the background plasma in keV. For example, this gives $I\lambda_L^2 \sim 10^{15}$ W/cm$^2 \cdot \mu$m^2 for $T_e \sim 1$ keV, and this value may explain the bending point of the hot electron scaling curve given in Fig. 2 in Ref. 4. Moreover, the hot electrons with their temperature $T_h \sim 8 \cdot T_e$ are estimated to be produced there through the acceleration by the wave field. It should, however, be noted that since the wave-breaking condition in the hot plasma is modified by the contribution of the partial trapping of the distribution function [14], the actual critical amplitude for wave-breaking must be lower than the above one.

The energy flux carried by the plasma wave out of the resonance region has been calculated with respect to absorption. For the driver with $V_d/V_{th} > 0.1$, the energy flux of the wave is found to exceed the free-streaming heat flux of the background electrons. At the same time, the hot electrons are expected to appear in this regime as shown in Fig. 9. In the situation where the density structure is strongly modified in a self-consistent manner by the ponderomotive force, it is also found that the local absorption model does not provide the strictly estimated absorption fraction.

Finally, the authors would like to make some physical comments on the wave-breaking regime. In the case where wave-breaking does not occur, the plasma wave amplitude increases sufficiently as the driver field increases,and the corresponding hot electron temperature increases sufficiently. However, once wave-breaking takes place, strong dissipation plays an important role in resonance absorption, and the wave amplitude is limited by this dissipation. As a result, the hot electron temperature does not increase [4] so much as before. In this wave-breaking regime, therefore, the formulation of the dissipation term, which should be a function of the wave amplitude, phase velocity, and the electron thermal velocity, becomes the essential problem. In addition to the wave amplitude limitation, the strong

dissipation may cause the spatial growth of the wave amplitude in the resonance region to reduce. As a result, spatial extension of the resonance region and an increase of the corresponding density scale length may be expected in this regime, possibly explaining the experimental results [16]. It should, however, be noted that the surface rippling arising from the two-dimensional instability is also a candidate for causing such broadening of the density scale. It is expected to solve the resonance absorption in this high-power regime by correctly modelling the damping term in the wave equation.

Acknowledgements

The authors would like to thank Dr. Witkowski for continuous interest and encouragement.
They greatly acknowledge many useful discussions with Dr. M. Kono.

References

1) J.P. Freidberg, R.W. Mitchell, R.L. Morse, and L.I. Rudsinski, Phys.Rev.Lett. 28, 795 (1972)

2) D.W. Forslund, J.M. Kindel, K. Lee, E.L. Lindman, and R.L. Morse, Phys.Rev. A 11, 679 (1975)

3) K.G. Estabrook, E.J. Valeo, and W.L. Kruer, Phys. Fluids 18, 1151 (1975)

4) D.W. Forslund, J.M. Kindel, and K. Lee, Phys.Rev.Lett. 39, 284 (1977)

5) K. Estabrook and W.L. Kruer, Phys.Rev. Lett. 40, 42 (1978)

6) G.J. Morales and Y.C. Lee, Phys.Rev.Lett. 33, 1016 (1974)

7) G.J. Morales and Y.C. Lee, Phys.Fluids 20, 1136 (1977)

8) K. Lee, D.W. Forslund, J.M. Kindel, and E.L.Lindman, Phys. Fluids 20, 51 (1977)

9) P.Mulser and C. van Kessel, Phys.Rev.Lett. 38, 902 (1977)

10) D. Sarafyan, Journal of Mathematical Analysis and Applications 40, 436 (1972)

11) A.Y. Wong, "Electromagnetic wave interactions with inhomogeneous plasmas", in Laser Interaction and Related Plasma Phenomena Vol. 4 (Plenum, N.Y. 1977)

12) M.A. Antosiewicz in Handbook of Mathematical Functions, edited by M. Abromowitz and I.A. Stegun (Dover, N.Y. 1970), p. 444

13) P. Koch and J. Albritton, Phys. Rev.Lett. 32, 1420 (1974)

14) W.L. Kruer, Phys. Fluids 22, 1111 (1979)

15) C.P. DeNeef and J.S. DeGroot, Phys. Fluids 20, 1074 (1977)

16) R. Fedosejevs, M.D.J. Burgess, G.D. Enright, and M.C. Richardson, Phys. Fluids 24, 537 (1981)

Figure Captions

Fig. 1 The relation between the Mach number M of the ion flow and the wave energy density in the form $\frac{1}{2}(A_s^2 - |A|^2)$ given in eq. (11). For the same value of the wave amplitude there are two roots in the Mach number, one being subsonic and the other supersonic.

Fig. 2 Schematic of symmetric part of the two-dimensional potential given in eq. (14) as a function of X (Y = 0). This structure depends on the parameters ρ_s and A_s.

(a) Schematic of U_s in the subsonic region.

(b) Schematic of U_s in the supersonic region.

Fig. 3 The resultant wave structures and the self-consistent density profile for the case with $A_s = 2$ and $\delta = 0.2$, and the corresponding driver strength $A_d = 0.32$.

(a) The density profile ($\rho = \rho_s/M$) and the ponderomotive potential profile ($\Phi = |A|^2/4$).

(b) The spatial structures of the wave field. The solid and dotted lines correspond to the real and imaginary parts of the field A, respectively.

(c) The phase space diagram of the wave field.

Fig. 4 The wave and density structures for the case with partial reflection assumed at the underdense boundary. The parameters used are $A_s = 3$ and $\delta = 0$, and 20 % reflection is assumed. The corresponding driver strength $A_d = 0.3$ is found.

(a) The density profile ($\rho = \rho_s/M$) and the ponderomotive potential profile ($\Phi = |A|^2/4$).

(b) The spatial structures of the wave field. The solid and dotted lines correspond to the real and imaginary parts of the field A, respectively.

(c) The phase space diagram of the wave field.

Fig. 5 (a) The maximum value of the electron quivering velocity (V_{os}) divided by the electron thermal velocity (V_{th}) as a function of the driver strength (V_d/V_{th}). This quantity $(V_{os}/V_{th})^2$ is equal to the ratio of the wave energy density to the electron thermal pressure at the critical density.

(b) The density scale length at the critical density as a function of the driver strength

Fig. 6 The densities of the upper density shelf ($n_1/n_{cr} = \rho_1$) the lower density shelf ($n_2/n_{cr} = \rho_2$), and the sonic point ($n_s/n_{cr} = \rho_s$) as functions of the driver strength.

Fig. 7 The peak value of the perturbed electron density associated with the resonantly excited plasma wave as a function of the driver strength. The dotted line shows its mean value.

Fig. 8 The solid line shows the energy flux carried by the plasma wave out of the resonance region as a function of the driver strength, while the dotted line shows the absorbed energy flux calculated with the local absorption model. The energy fluxes are normalized by the free-streaming limit of the electron heat flux at the critical density.

Fig. 9 The hot electron temperature as a function of the driver strength. T_h is estimated by means of the standing-wave model presented in Ref. 15.

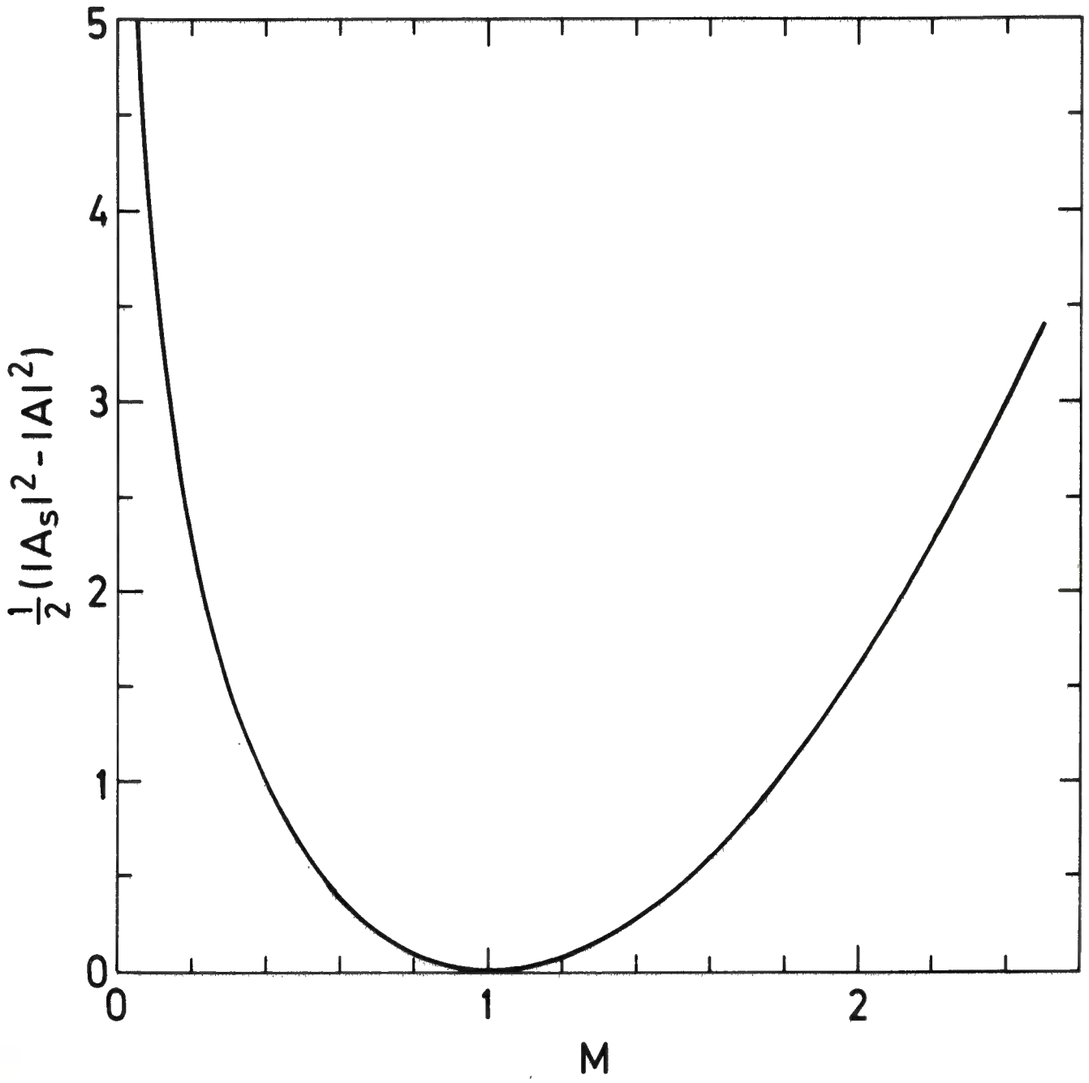

Fig. 1

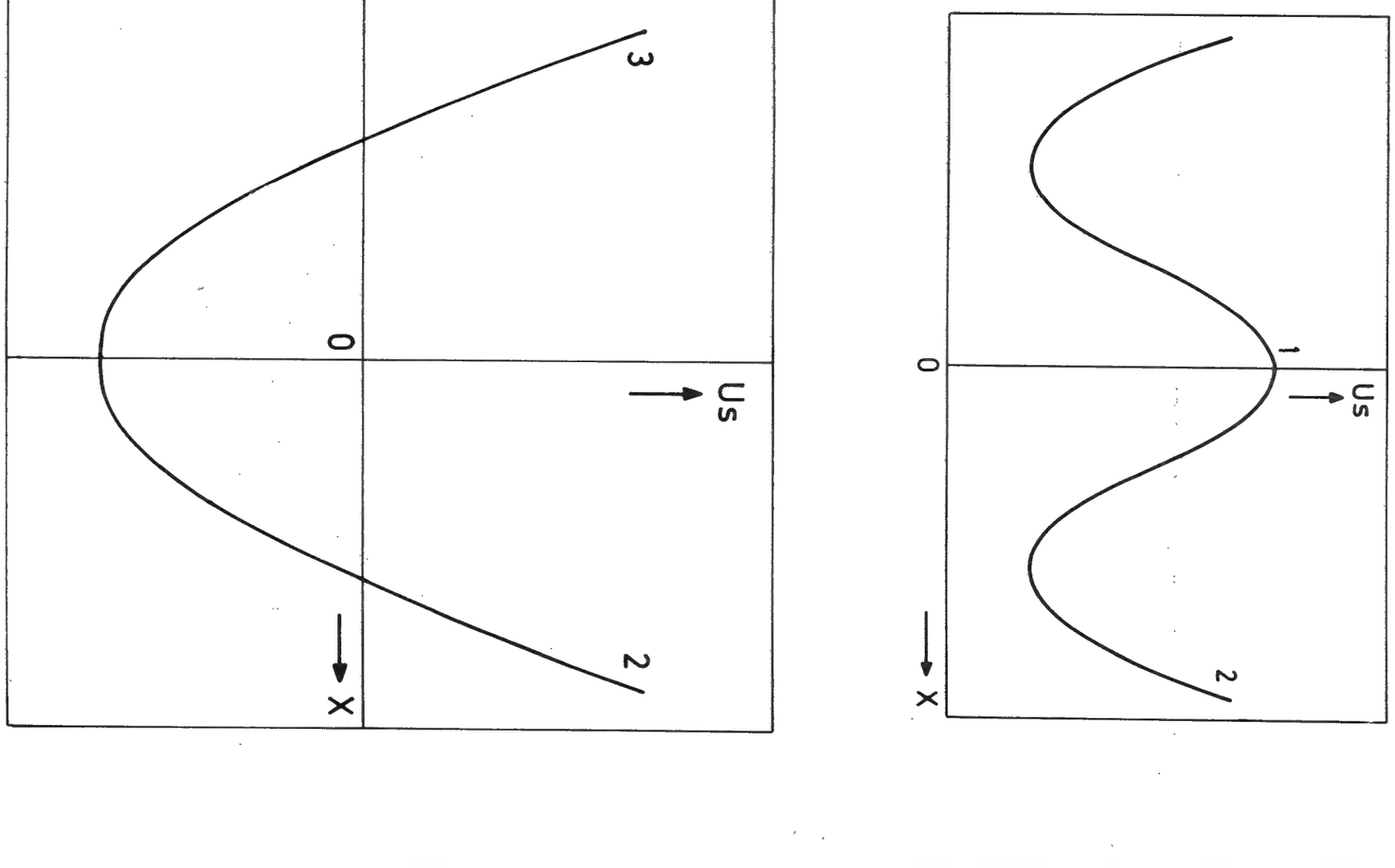
a)
Us
1
0
X
2
b)
3
Us
0
2
X

Fig. 2

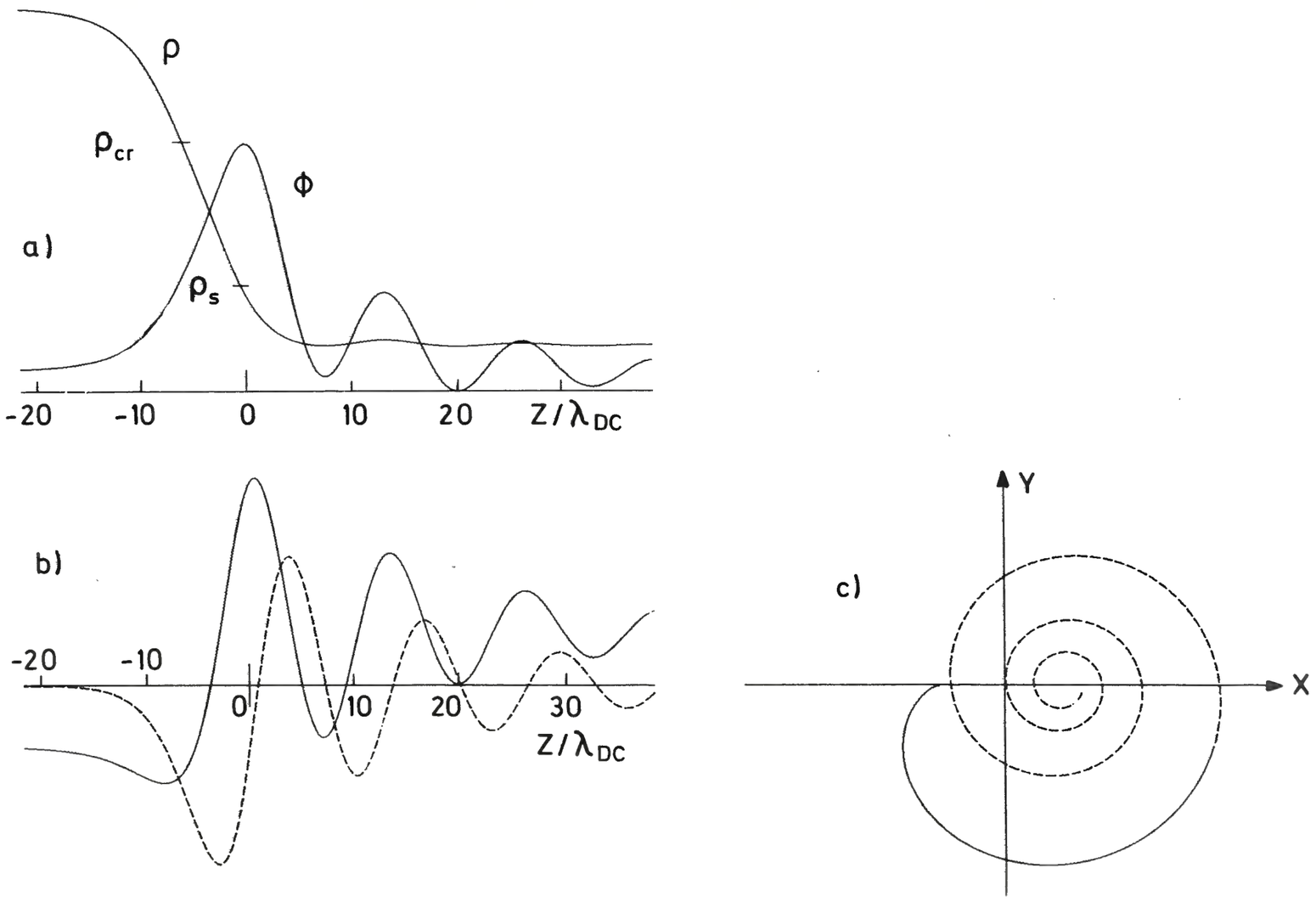
ρ
ρcr
Φ
a)
ρs
-20
-10
0
10
20
Z/λDC
b)
-20
-10
0
10
20
30
Z/λDC
c)
Y
X

Fig. 3

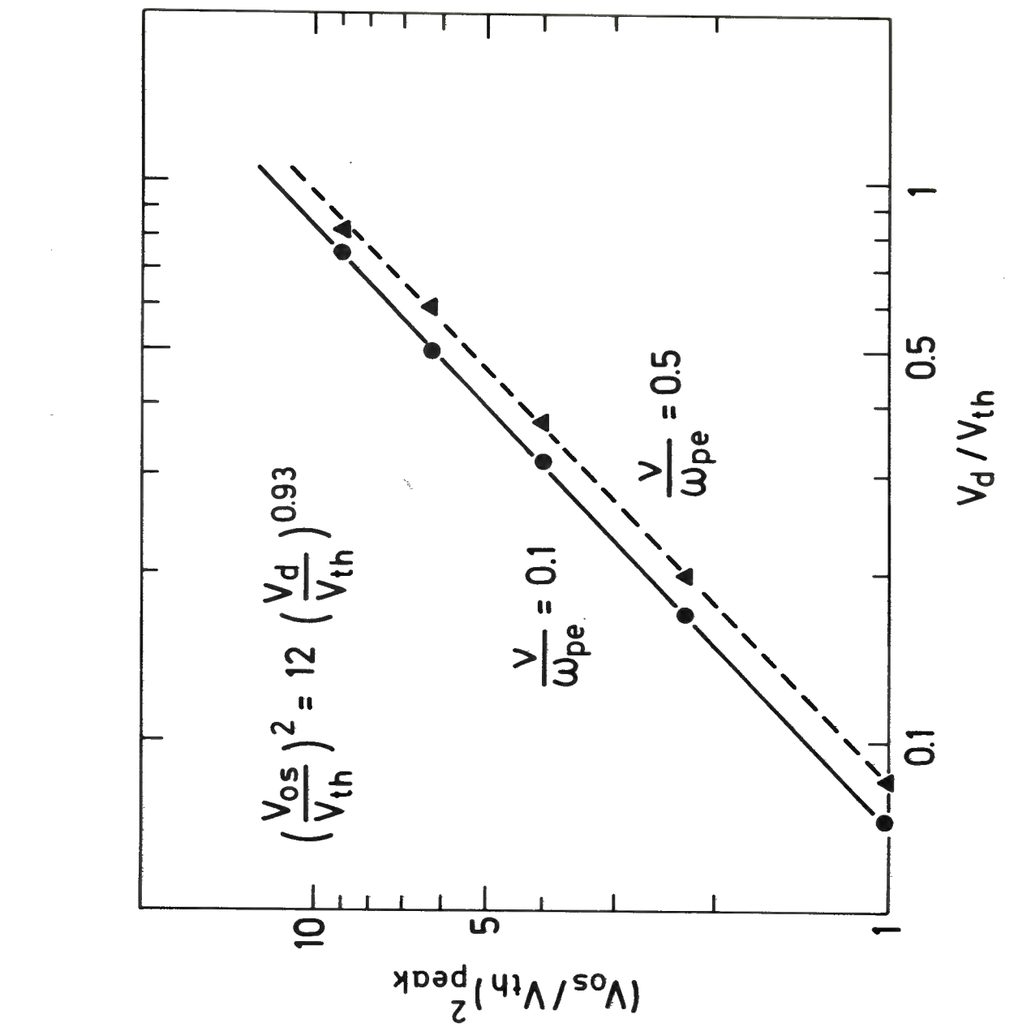
$(\frac{V_{os}}{V_{th}})^2 = 12\,(\frac{V_d}{V_{th}})^{0.93}$
$\frac{\nu}{\omega_{pe}} = 0.1$
$\frac{\nu}{\omega_{pe}} = 0.5$
$(V_{os}/V_{th})^2_{peak}$
10
5
1
0.1
0.5
1
V_d / V_{th}

Fig. 5 (a)

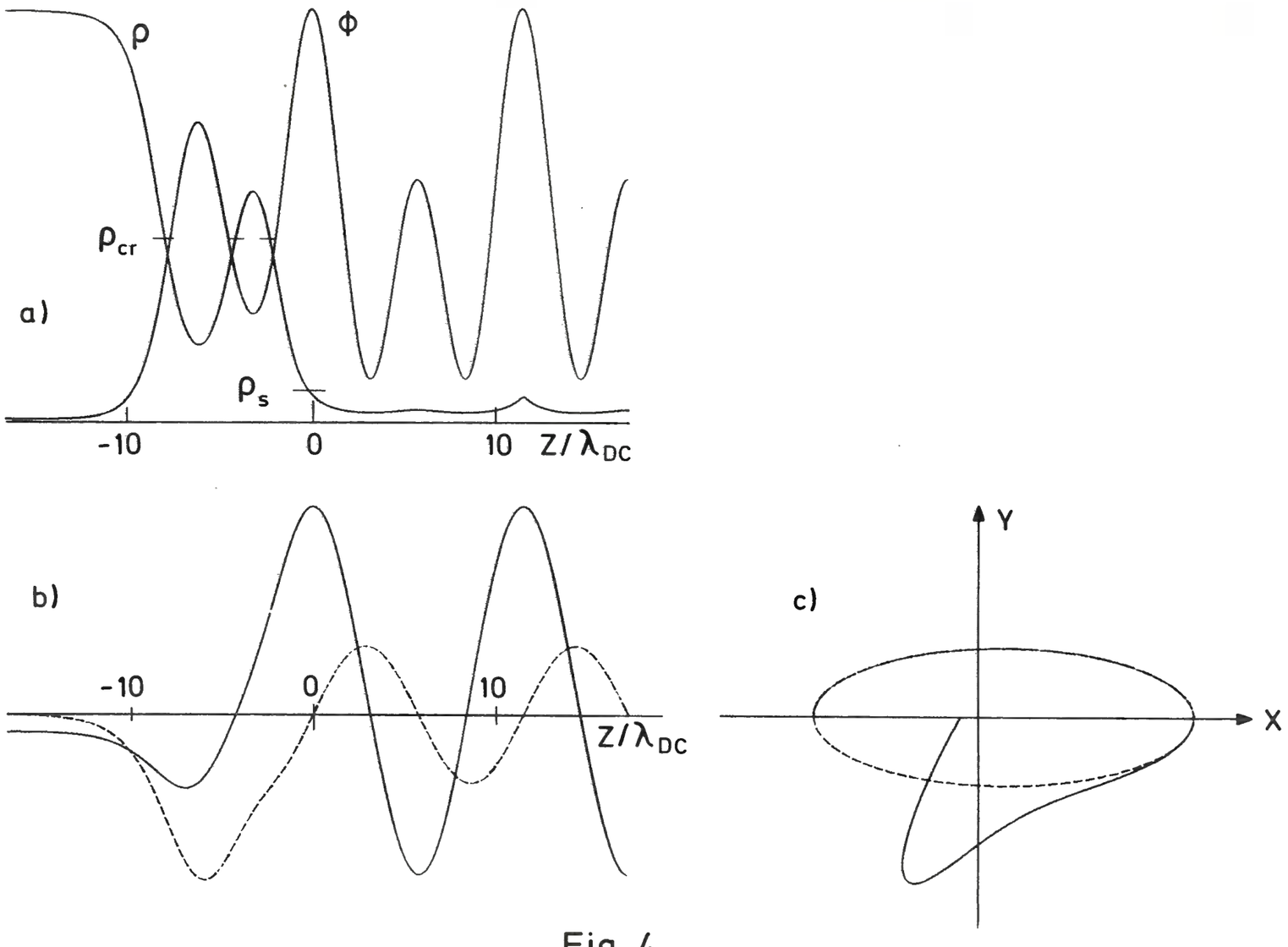
a)
ρ
Φ
ρ_{cr}
ρ_s
-10
0
10
Z/λ_{DC}
b)
-10
0
10
Z/λ_{DC}
c)
Y
X

Fig. 4

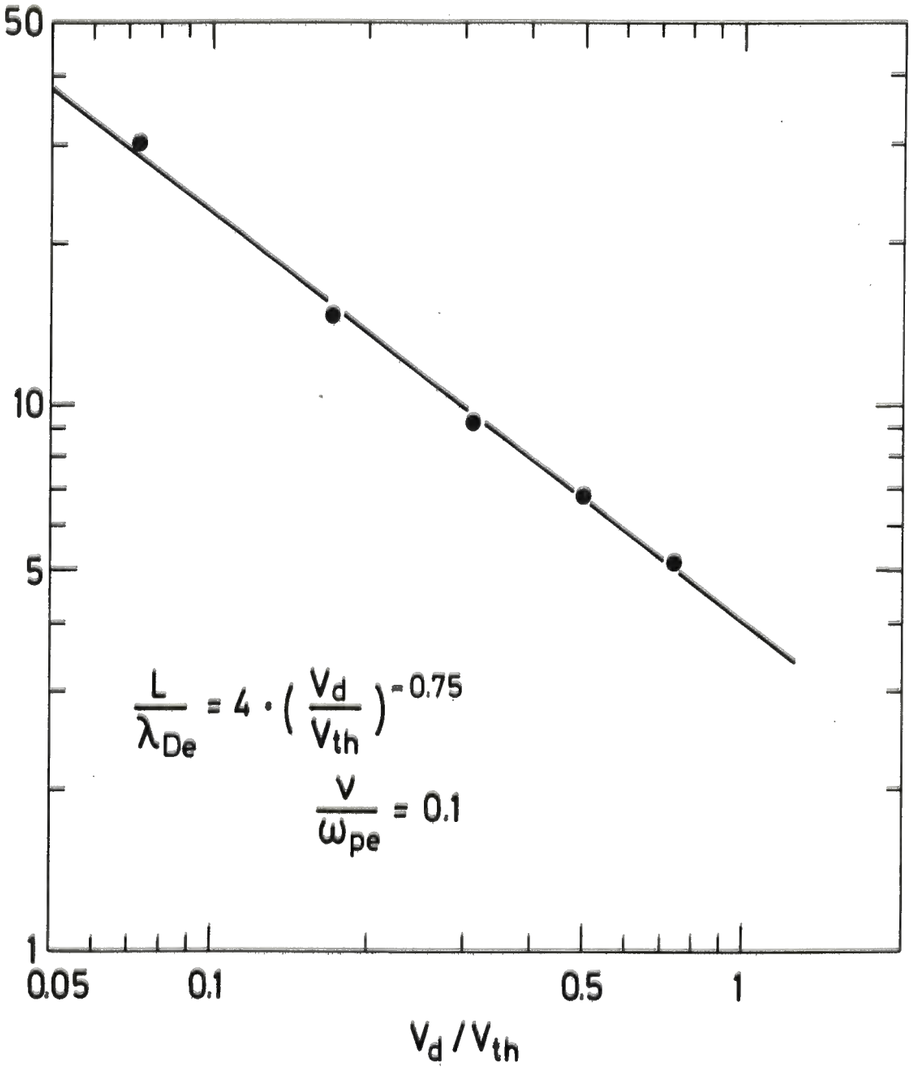
50
10
5
1
0.05
0.1
0.5
1
L/λDe
L/λDe = 4 · (Vd/Vth)^-0.75
ν/ωpe = 0.1
Vd / Vth

Fig. 5 (b)

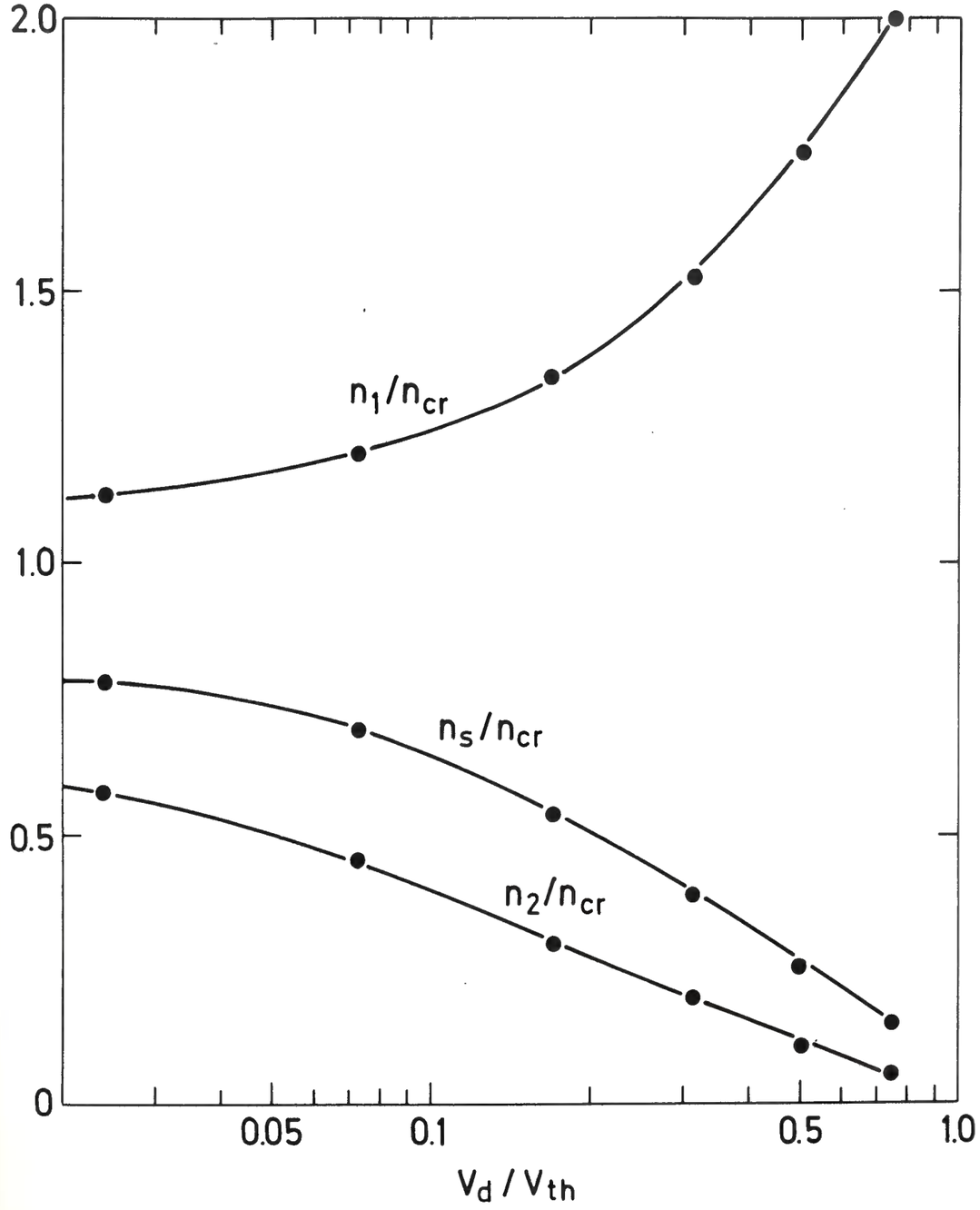
2.0
1.5
1.0
0.5
0
n1/ncr
ns/ncr
n2/ncr
0.05
0.1
0.5
1.0
Vd / Vth

Fig. 6

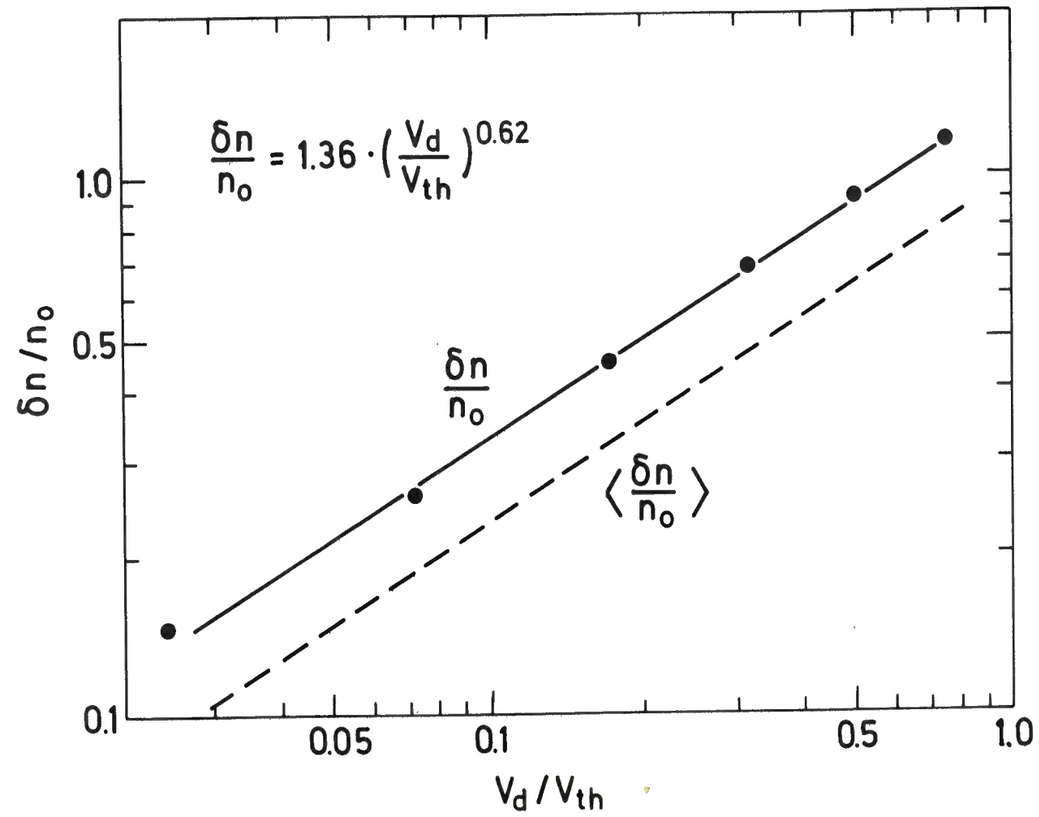
$\frac{\delta n}{n_o} = 1.36 \cdot \left(\frac{V_d}{V_{th}}\right)^{0.62}$
1.0
0.5
0.1
$\delta n / n_o$
$\frac{\delta n}{n_o}$
$\langle \frac{\delta n}{n_o} \rangle$
0.05
0.1
0.5
1.0
V_d / V_{th}

Fig. 7

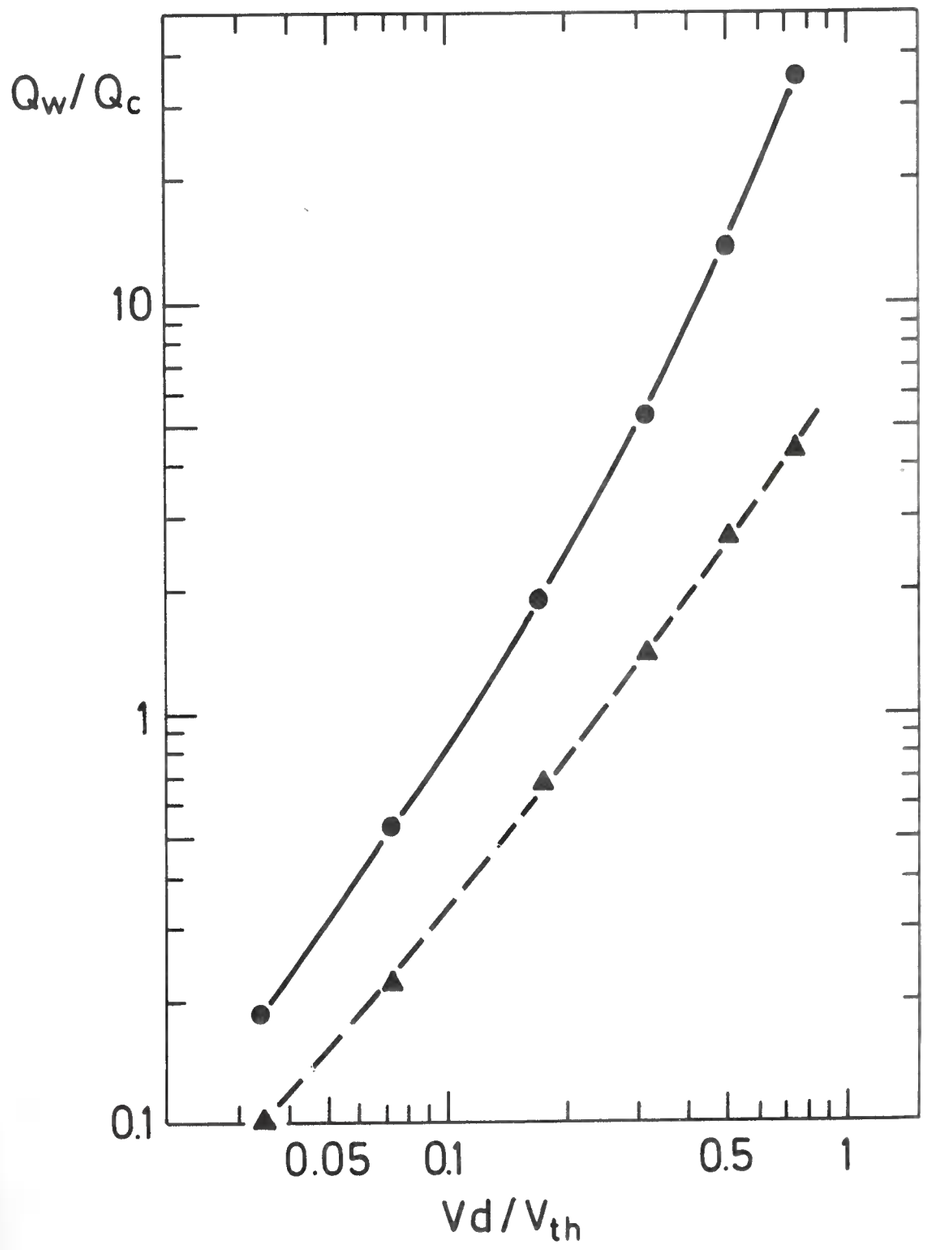
Q_w / Q_c
10
1
0.1
0.05
0.1
0.5
1
Vd / V_{th}

Fig. 8

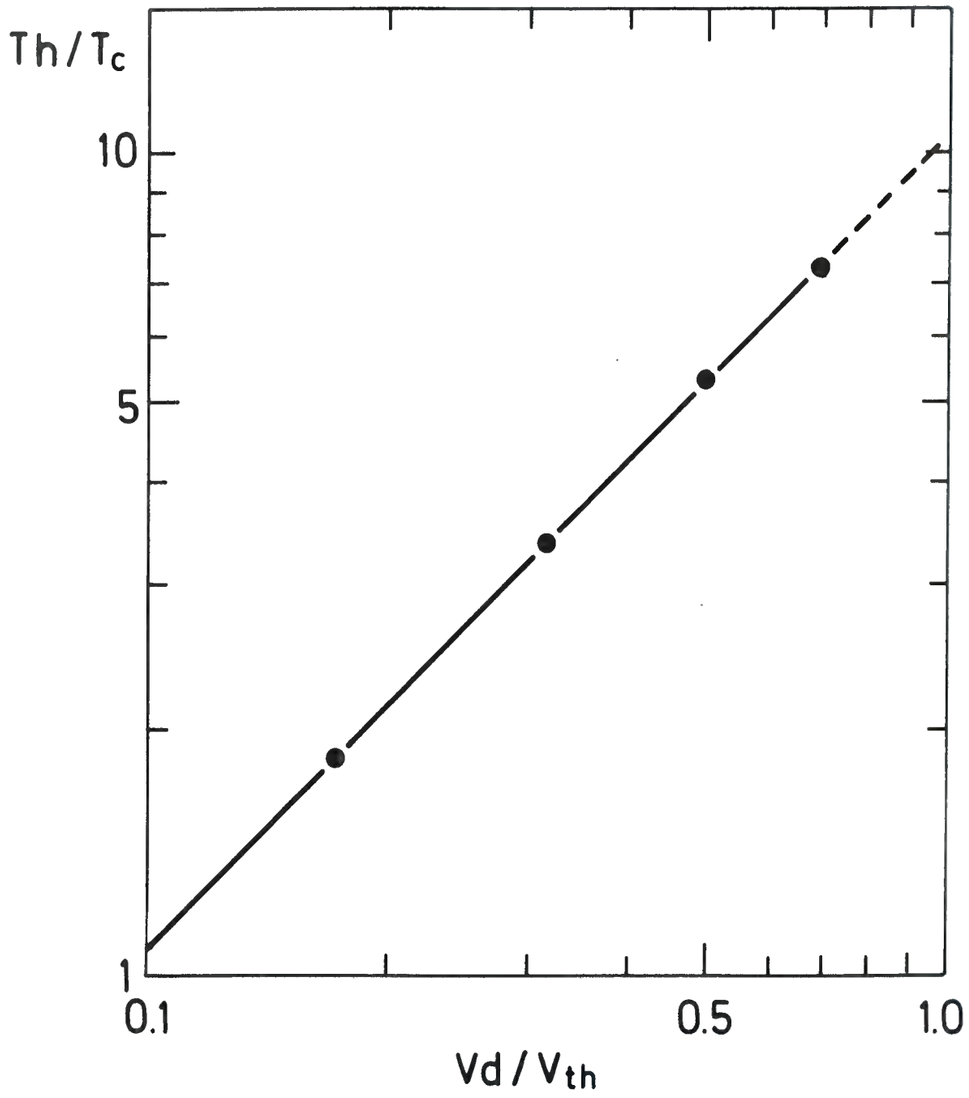

Fig. 9